Cent. Eur. J. Geosci. • 5(3) • 2013 • 374-386
DOI: 10.2478/s13533-012-0138-3

VERSITA

Central European Journal of **Geosciences**

Sequence Stratigraphic Analysis and Integrated 3D Geological Modeling of M1 Block, Wenmingzhai Oilfield, Dongpu Depression, China

Research Article

Xue Li[1]*, Jinliang Zhang[1†], Yong Yuan[2], Cunlei Li[3], Ningning Meng[2]

1 *College of Resources Science & Technology, Beijing Normal University, Beijing 100875, China*

2 *College of Marine Geosciences, Ocean University of China, Qingdao 266100, Shangdong, China*

3 *College of Geological Science and Engineering, Shandong University of Science and Technology, Qingdao 266500, Shangdong, China*

Received 26 May 2013; accepted 15 August 2013

Abstract: The M1 block is a typically complex fault-block oilfield, whose recovery has reached 30.5% through the twenty years waterflooding development. Remaining oil scatters very widely and the production between layers is in a high degree. However, many problems have been exposed at the same time which hinder improvement of the recovery rate and sustainable development of the reservoir. Hence, it is important to carry out basic geological research and form a comprehensive understanding of reservoir properties. However, few such studies have been conducted in China. In this study, work related to basic geological research was conducted based on high-resolution sequence stratigraphy, seismic interpretation technology and 3D visual geological modeling, and significant results were achieved. Three sequence orders and three types of interfacies in the stratigraphic architecture of M1 block were identified through seismic sections, logging curve characteristics and entropy spectrum analysis. Thirty-two short-term sequence cycles (fifth order), eight mid-term sequence cycles (fourth order) and two long-term sequence cycles (third order) were identified, followed by the establishment of a high-resolution isochronous stratigraphic correlation framework. Finally, a regional 3D geological model was established on the basis of these preliminary studies. The integrated 3D geological model is a valuable tool for reflecting geological bodies accurately, and it can accurately represent and describe reservoir heterogeneity.

Keywords: Seismic interpretation • High-resolution sequence stratigraphy • Sequence cycle • 3D Geological Modeling • Shahejie forrmation.

1. Introduction

Sequences are defined as relatively conformable successions of genetically related strata bounded by unconformities or their correlative conformities [1]. Strata within

*E-mail: lix@mail.bnu.edu.cn
†E-mail: jinliang@bnu.edu.cn

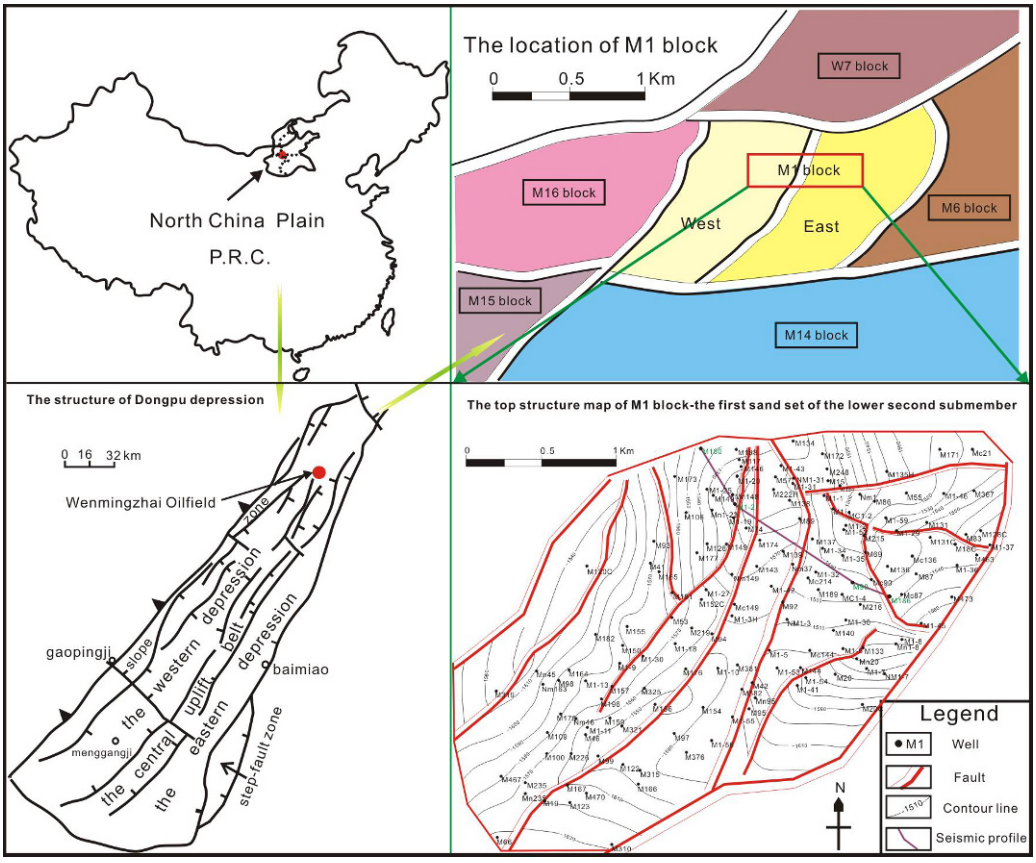

Figure 1. Location map of Wenmingzhai Oilfield, showing the main area and faults of the M1 block.

sequences display predictable changes in their stacking patterns through time, which relates to the subdivision of sequences into systems tracts. Sequence stratigraphy, a sub-discipline of stratigraphy dealing with the genetic interpretation of lateral and vertical facies changes of a basin-fill, is the study of facies changes within a time framework. Sequence stratigraphic analysis assumes a subdivision of the sedimentary pile into sequences, which are stratigraphic units related to cyclic changes in the sedimentation regime through time [2]. The complex architecture and heterogeneity of the strata units and numerous stratigraphic hiatuses cause difficulty for stratigraphic interpretations. This highlights the importance of using high-resolution sequence stratigraphy to reconcile these problems.

Geological modeling has a wide application in oilfields all over the world. However, conventional modeling just uses the structural map provided by the oilfield rather than reinterpreting it with seismic data, and cannot combine the shape of sand bodies with surrounding structural layers [3, 4]. In order to make geological modeling more reasonable, increasing the exactitude and decreasing the uncertainty has become the focus of studies for reservoir description and geological modeling nowadays [5]. In this paper, an integrated 3D geological model of the M1 block has been constructed, particularly, the information contained in the 3D seismic interpretation of small faults has been used to reduce uncertainty. The 3D geological model comprehensively considers the effects of structural condition and sequence stratigraphy, and efficiently characterizes the geological characteristics of the M1 block.

2. Regional Setting

Wenmingzhai oilfield lies at the junction of Qingfeng County of He'nan Province and Shen County of Shandong Province, with its majority in the latter. As for structural position, this oilfield is located in the narrowest northern region of Dongpu depression (Fig. 1). Wenmingzhai oilfield, a complex and abundant fault-block oilfield, is controlled by two sets of NEE-trending faults in opposite trends. The reservoir is buried in 1360 m to 2320 m deep with an oil-bearing cover of 6.84 km^2. The M1 block, sep-

arated into the eastern part and the western part by the M25 fault in its middle, is located in the middle of Wenmingzhai Oilfield. The block is surrounded by the M6 block in the east, the M14 block in the south, the M16 block in the west and the W7 block in the north [6].

Shahejie Formation (Fm.) is divided into four members, in decreasing age order, Member 4 (ES4), Member 3 (ES3), Member 2 (ES2) and Member 1 (ES1). ES3 consists of three sub-members, the upper sub-member (S3U), the middle sub-member (S3M) and the lower sub-member (S3D), respectively. Other members are composed of the lower sub-member and the upper sub-member. S3U consists of three sand sets, the first sand set, the second sand set and the third sand set, named S3U1, S3U2 and S3U3, respectively, with increasing depth. S2D is composed of four sand sets, named S2D1, S2D2, S2D3 and S2D4 with increasing depth, respectively. The well-developed sandstone is mainly distributed in ES4, ES3 and ES2 with a cumulative thickness of 10 m to 60 m, and displays large lateral variations. The lower ES2, 180 m to 200 m thick, and the upper ES3, 220 m to 225 m thick, are target members for this study. The lower sub-member of ES2 is a section of interbeds composed of sandstone and mudstone. The color of the upper mudstone and the lower interbed is gray and purple, respectively. The sandstone is characterized by pure sandstone, little mudstone and high reservoir resistivity. Generally speaking, compared with other members, the physical properties of the lower sub-member of ES2 is better, with the characteristics of average porosity 27.89%, average permeability is 899.73 $\times$ 10^{-3} μm^2 and carbonate content 9.44%. The lithology of the upper sub-member of ES3 is interbedded dark gray shale, oil shale and sandstones. Sandbodies are mainly distributed in S3U1, S3U2 and S3U3 with stable transverse distribution, and the cumulative thickness is generally 50 m to 60 m.

The M1 block contains 77 fault blocks in an oil-bearing area of 3.9 km^2, with a fault density of 19.7 per km^2. Among all the fault blocks, the block area less than 0.1 km^2 accounts for 77.4%. There are so many regional fractures that it is difficult to figure out the changes of lithology and sandbodies, the spatial form of small faults, and the description of low-amplitude structures and staggered faults. As few related studies have been conducted in the M1 block, sequence stratigraphic analysis and fine 3D seismic interpretation are hereby given in this paper. Accordingly, the faults geometries and their spatial distributions are characterized, which can provide geological information for 3D geological modeling.

3. Recognition of Sequence Boundary and Division of Sequence Cycle

3.1. Recognition of sequence boundaries

Sequence stratigraphy is the study of genetically related facies within a framework of chronostratigraphically significant surfaces. The sequence is the fundamental strata unit for sequence stratigraphic analysis which is based on the identification of the smallest stratigraphy units or genetic stratigraphic units [7–10].

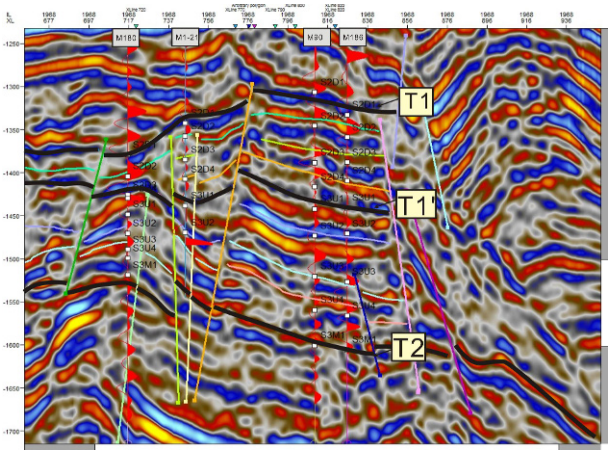

Figure 2. 3D seismic profile of well M180 - well M1-21 - well M90 - well M186, showing the sequence boundaries of target formations. T1: the top of the lower second sub-member (ES2); T1': the top of the upper third sub-member (ES3) ; T2: the bottom of the upper third sub-member (ES3).

3.1.1. Recognition of seismic interfaces

There are so many combination patterns and cross-cuttings between east-dipping fractures and west-dipping fractures making the structure of the target area complex. Though the lower second sub-member and the upper second sub-member of ES2 are both interbedded mud rock and sandstone, the former has obvious lateral alternation of sand bodies with various electrical characteristics, pure sandstone and high resistivity. Therefore, it is more reliable for the correlation between the two sub-members. The sequence boundary between the two sub-members is the T1 reflective surface. There is a set of relatively stable mudstone units with obvious electrical characteristics at the bottom of ES2, and this is the boundary from which the mudstone color becomes darker downward and oil shale begins to appear. This boundary is named T1' reflective surface, separating ES2 from ES3. T1 and T1' have obvious wave impedance interfaces and are both local unconformities. The T2 reflective surface, a regional unconformity, is the sequence boundary of the upper and

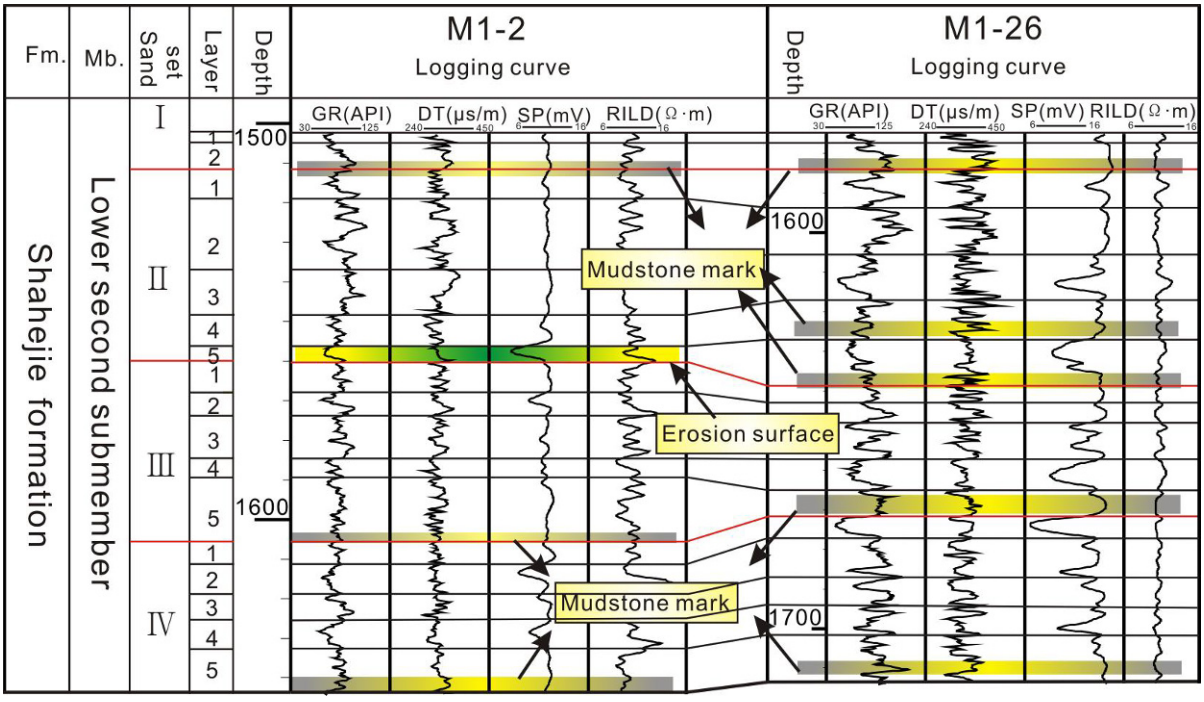

Figure 3. Logging characteristics of well M1-2 and well M1-26, showing the sequence boundary mark for the lower second sub-member (ES2) of Shahejie FM.. Fm. : Formation; Mb. : Member.

the middle third sub-member, displaying an obvious wave impedance interface and strong reflective energy, which can be successively tracked in the whole area, as shown in Figure 2. The surface names in Figure 2 represent the top position of formations. The T1 surface is the sequence boundary between the bottom of the upper second sub-member and the top of the lower second sub-member which consists of four sand sets: S2D1, S2D2, S2D3 and S2D4 with increasing depth, respectively. The T1′ surface is the sequence boundary between the bottom of the lower second sub-member and the top of the upper third sub-member which consists of four sand sets: S3U1, S3U2, S3U3 and S3U4 with increasing depth, respectively. The T2 surface is the sequence boundary between the upper third sub-member and the middle third sub-member. The surface names at each well top is to more clearly show the surface position. In previous studies of the regional sequence stratigraphy, no significant maximum flooding surfaces had been recognized in the study area.

3.1.2. Recognition of logging interfaces

Erosion surfaces, flood surfaces and mudstone marks can be identified from well logging [11, 12]. In general, erosion surfaces develop at the bottom of thick sandstone bodies with high-amplitude box-shaped or bell-shaped logging. Flood surfaces, the transformation of base level from rise to falling, are marked by the emergence of dark lacustrine mudstone units with straight spontaneous potential curves. The logging characteristics of mudstone marks are "three high and one low", that are high spontaneous potential (SP), high natural gamma (GR), high acoustic time (DT) and low density, which can be easily identified from sections [13]. However, no significant maximum flooding surfaces develop in the study area. Only two interfaces, mudstone marks and erosion surface, develop in the target member, which are directly recognized from logging curves based on logging response of different marks.

Taking well M1-2 and well M1-26 for example, mudstone marks are identified at the bottom of each sand set of well M1-26 (Fig. 3). A total of eight mudstone marks are identified from logging curves of well M1-2 and well M1-26. Erosion surfaces generally develop at the bottom of the sandstone, and are located at the bottom of box-shaped or bell-shaped SP curve with a low resistivity curve. Also, erosion surfaces are seen as the transformation of base level from falling to rising. In the study area, erosion surfaces develop between the second sand set and the third sand set with high-amplitude bell-shaped or funnel-shaped natural gamma and spontaneous potential curves, which can be as the sequence boundary of these two sets, as shown in well M1-2 (Fig. 3).

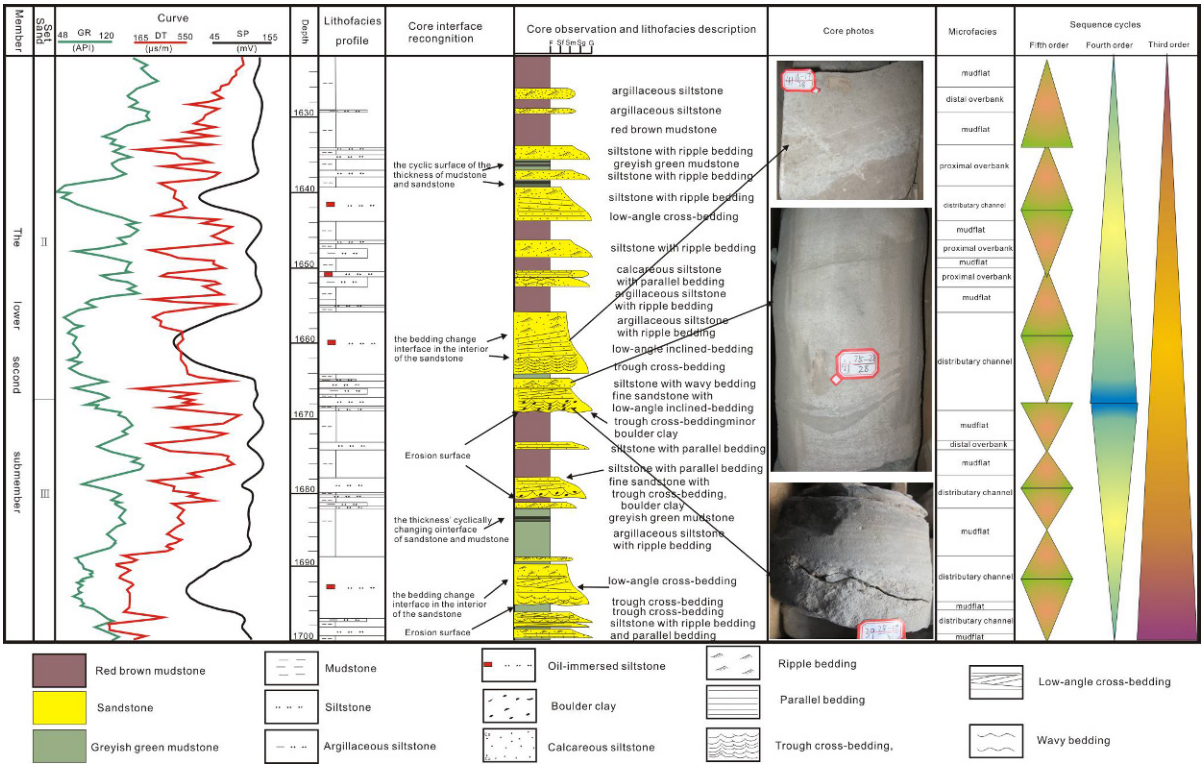

Figure 4. Schematic sections of well M49 at different studied layer of the lower second sub-member (ES2) ; the section shows the sediments, deposition bedding structures and depositional sequence cycles; and three kinds of core interfaces are recognized. F, Sf, Sm, Sg, G represent mudrock, fine sandstone, medium sandstone, coarse sandstone and gravel, respectively.

3.1.3. Recognition of core interface

Through detailed core observation and description, three types of core interfaces are recognized, erosion surfaces, the bedding change interfaces and the thickness cyclic changing interface of sandstone and mudstone, respectively.

It can be observed from core wells of the M1 block that there are erosion surfaces at the bottom of distributary channels of terminal fans or shallow-water delta fronts. Erosion surfaces result from strong currents when they flow through unconsolidated deposition surface causing uneven surfaces (Fig. 4). The top of the erosion surface is the place where many boulder clay and lag deposits are encountered.

The bedding change interface has a wide distribution in the study area and it is the reflection of hydrodynamic change during the formation of sediments. Taking well M49 for example, the change from trough cross-bedding to cross-bedding to ripple bedding (Fig. 4) reflects the increasing depth of water and expanding accommodation which can be seen as a retrograding cycle indicating the rise of the base level. Conversely, the bedding change from ripple bedding to cross-bedding to trough cross-bedding reflects the decreasing depth of water and the increasing hydrodynamic force which is the indication of base level falling.

The thickness cyclic changing of sandstone and mudstone is also related to hydrodynamic force and base level. The decrease in sandstone thickness and the increase in mudstone thickness accordingly reflect the decrease of the hydrodynamic force and the rise of base level. Additionally, the increase in sandstone thickness and the decrease in mudstone thickness indicates the increase of the hydrodynamic force and the falling of base level (Fig. 4).

3.2. Division of sequence cycles

Three sequence orders are identified in the stratigraphic architecture of the M1 block through core observation and description, fifth-order (V) short-term sequence cycle, fourth-order (IV) mid-term sequence cycle and third-order (III) long-term sequence cycle [14], respectively. Taking well M49 for example, based on the analysis of stacking patterns of short-term sequence cycles combined with determination of mid-term sequence cycle sequence interfaces, thirty-two short-term sequence cycles, eight mid-

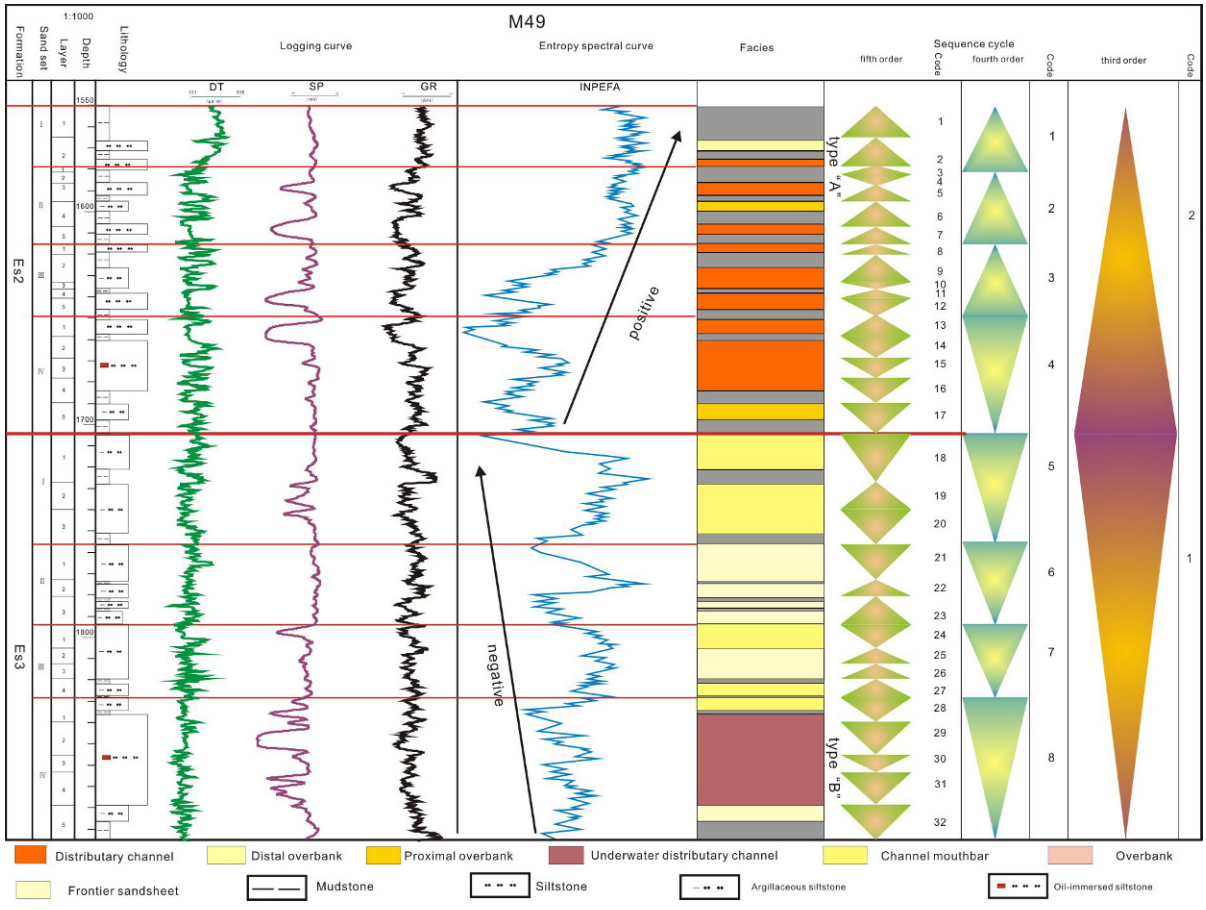

Figure 5. The division scheme of sequence stratigraphy of the M1 block, showing the types of short-term cycle and the main cycle trend of the lower second sub-member and the upper third sub-member, which are a positive trend and a negative trend, respectively.

term sequence cycles and two long-term sequence cycles are identified (Fig. 5).

Geological data for identifying short-term sequence cycle are generally cores and lithological sequences. The boundary of short-term sequence cycles are typically the erosion surfaces at the bottom of sand bodies [15, 16]. There are mainly two types of short-term sequence cycles in the M1 block, upward-deepening asymmetric sequences (type "A") and upward-shallowing asymmetric sequences (type "B"), respectively.

The mid-term base level cycle is composed of two to five superimposed short-term sequence cycles with a certain combination and arrangement. The fourth-order mid-term cyclic sequence, a subdivision of the third-order long-term cyclic sequence, has a relatively complete cycle structure forming in the process of regional transgression or regression. In this paper, we determine the stacking patterns according to the changes and the vertical combination of GR, SP, the density curves and resistivity curves. Taking No.7 and No.8 mid-term cyclic sequences for example (Fig. 5), the GR and SP become smaller upward, indicating the decreasing water depth and the corresponding facies change from distributary channel to channel mouth-bar or from frontier sand-sheet to channel mouth-bar. These two mid-term cyclic sequences are reverse cycles. On the contrary, the upward increase of GR and SP readings indicates an increase of mudstone and a decrease of sandstone, showing the rise of base level, such as No.1 and No.3 mid-term cyclic sequences which are both positive cycles with the sedimentary facies changing from distributary channel to proximal overbank to distal overbank.

Factors that control long-term cyclic sequences are the intensity of secondary structures and the change of base level affected by long periodic changes in secondary structure activity [17, 18]. The long-term cyclic sequence is defined as third-order sequence cycle (III) because of its long time span, and the sequence boundary of third-order sequence cycles are tectonic unconformity, large erosion surfaces and lithological mutation surfaces. A third-order long-term cycle composed of the superposition of several

fourth-order mid-term cycles represents a large-scale regional transgression or regression with deposition hundreds of meters thick, and its development and structure are mainly controlled by the tectonic background of sedimentary basins which are different from that of mid-term and short-term cycles. Two third-order long-term cycles are identified in the M1 block based on well logging, sedimentary character and the stacking pattern of mid-term cycles. The No.1 long-term cycle, composed of No.5 to No.8 mid-term cycles, is half of a long-term fall in base level. During late ES3 deposition, the activity of Lanliao fault which controls basin subsidence weakens, meanwhile, the climate changes from humid to arid. These phenomena probably indicate a wholesale tectonic uplift leading to a fall in lake level and decrease in water cover, thus a shallow delta system is formed in the upper third sub-member.

The No.2 long-term cycle consists of No.1 to No.4 mid-term cycles and it is half of a long-term base level rise, mainly forming in an arid environment. From INPEFA (a curve representing the trend of spectral properties and reflecting the major trend of cycles), it can be seen that the main trend of base-level change for the lower second sub-member is positive, displaying a transgression deposition, while the upper third sub-member is just opposite, showing a regression deposition, as shown in Figure 5.

According to the results of sequence division and sedimentary environment analysis, the top and the bottom of mid-term cycles and erosion surfaces are chosen as the framework of isochronous stratigraphic correlation, and the short-term cycle is chosen as the unit for isochronous stratigraphic correlation based on the principles of sequence stratigraphy and the characteristics of all sequence cycles. Then two sets of cross-well sections that can control the regional sequence stratigraphy are drawn, that are north to south profile (Fig. 6) and east to west profile (Fig. 7), and the high-resolution sequence stratigraphic correlation framework of the M1 block is built accordingly.

4. Detailed Structural Interpretation

4.1. Calibration and tracking of horizons

4.1.1. Synthetic seismograms

A synthetic seismogram is a bridge for connecting seismic data and geology [19]. The first step is to calculate the start-time of well logging with integrated speed, then the wave impedance and reflection coefficient are calculated with DT and density curves, and the theogram demarcation is achieved accordingly, by extracting the seismic wavelet from the well profile and get the result by convolving this wavelet with the wave impedance and reflection coefficient.

In this paper, sliding technology is used and the correlation coefficient is calculated by theogram sliding at a relatively small step. The seismic geological position is reasonable and accurate until the correlation coefficient reaches the maximum. The correlation coefficient of the synthetic seismogram for the M1 block is about 0.7 and the dominant frequency of the lower second sub-member and the upper third sub-member is in the range of 30 to 40 Hz, which has met the requirements of acoustic impedance inversion. Taking well M90 for example, the synthetic seismograms are eventually produced by extracting the seismic wavelet, and the simulated parameters were modified with repeated investigation and adjustments.

The comparison between various information and seismic profiles makes DT accord with depth relationships, key single well depth profiles accord with regional comprehensive speed, the regional standard layering accord with the specific geological reflective layers, and ultimately synthetic seismogram is achieved.

4.1.2. Calibration and interpretation of horizons

On basis of synthetic seismograms, seismic well correlation profiles are selected to make horizon interpretations [20]. Backbone profiles and seed points which can control regional change of horizons and faults are chosen to create the horizon tracking and explanation. From the seismic profile (marked with blue line in Fig. 1), it can be seen that the first three sand sets of the lower second sub-member (S2D1, S2D2, S2D3) and the second sand set of the upper third sub-member (S3U2) have relatively strong reflection energy and more obvious geological information. T1, the top interface of the lower second sub-member, is a group of high amplitude reflections and a standard horizon. Sand bodies of the first sand set of the upper sub-member (S3U1) are relatively thin, but large set of mudstone interlayers are developed. The top of S3U1 is a group of peak reflections, while the reflection coefficient of this interface is negative. The bottom corresponds to a trough reflection with a negative reflection coefficient. T2, the bottom interface of the upper third sub-member or the top interface of the middle third sub-member (S3M1), has a group of high amplitude reflections and a positive reflection coefficient. The interfaces between zones are accurately calibrated on the seismic section by means of synthetic seismogram (Fig. 8).

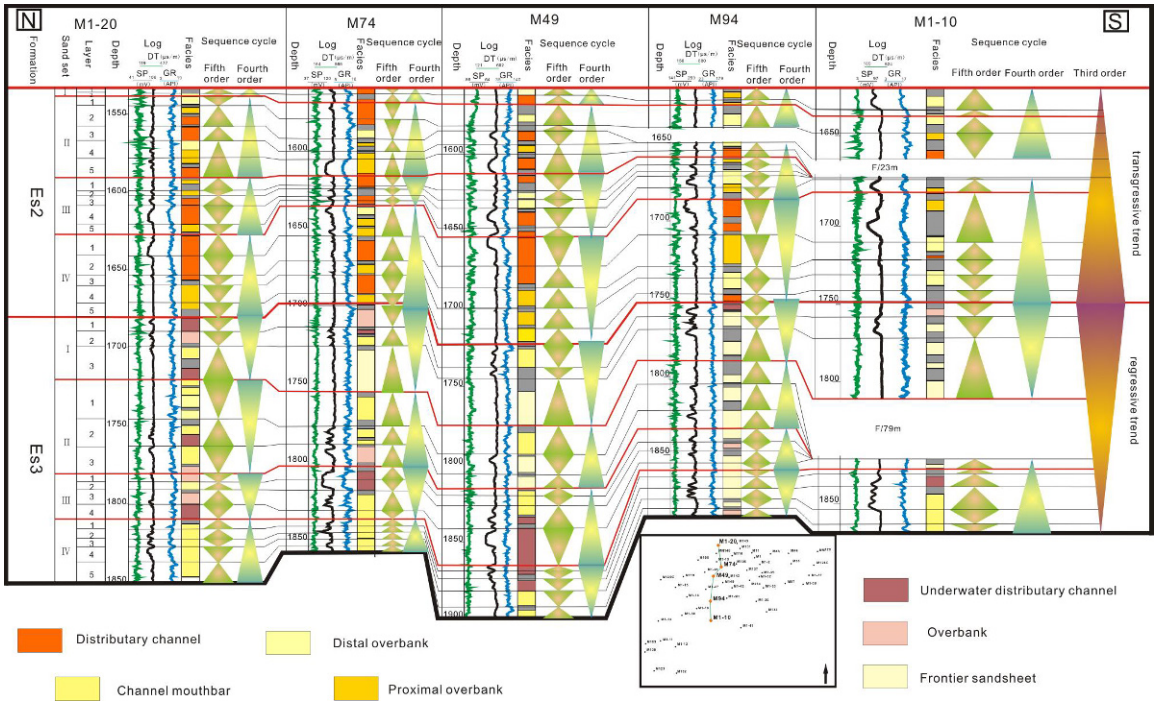

Figure 6. The north-south high-resolution isochronous stratigraphic correlation framework of well M1-20 - well M74 - well M49 - well M94 - well M1-10, displaying the correlation and division of sequence cycles of the lower second sub-member and the upper third sub-member, and the changes of water depth and sediments.

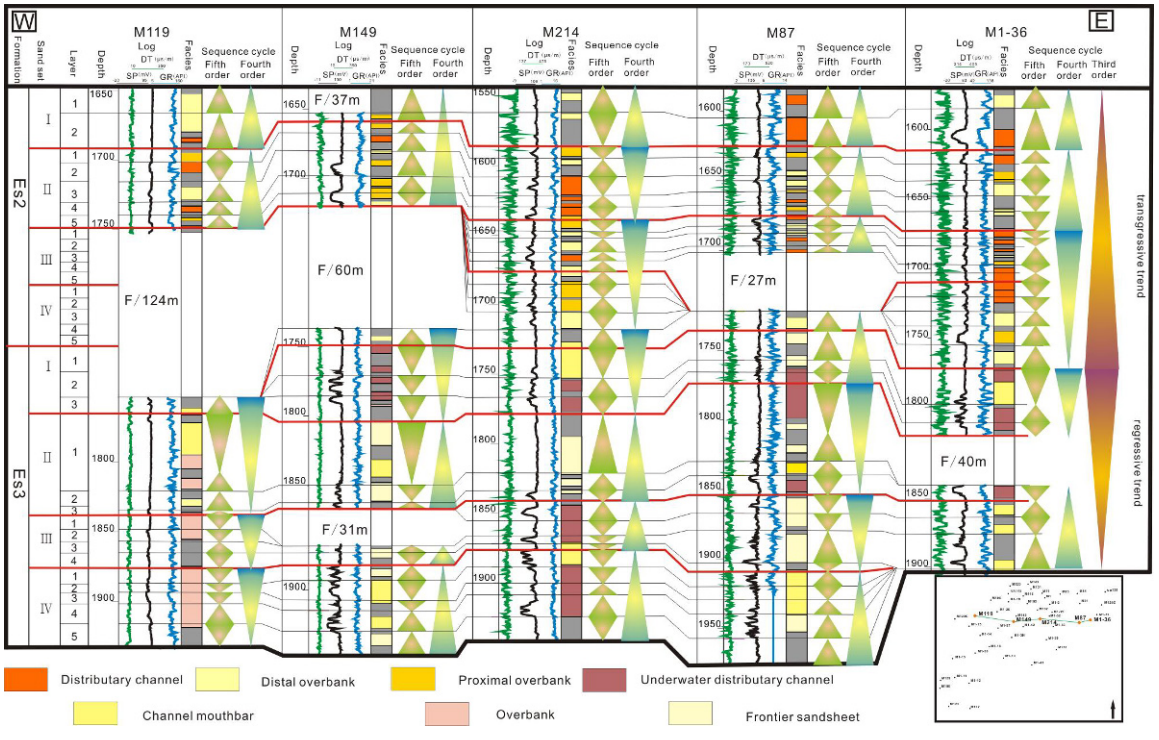

Figure 7. The west-east high-resolution isochronous stratigraphic correlation framework of well M119 - well M149 - well M214 - well M87 -well M1-36, displaying the correlation and division of sequence cycles of the lower second sub-member and the upper third sub-member of Shahejie Fm., and the changes of water depth and sediments.

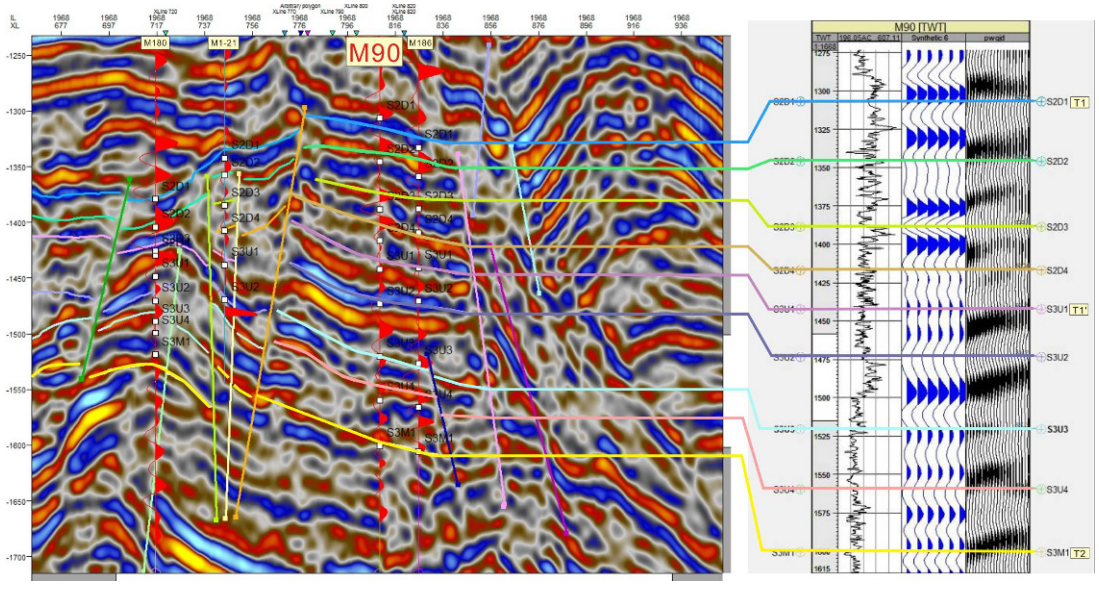

Figure 8. 3D seismic profile of well M180 - well M1-21 - well M90 - well M186, and the synthetic seismogram of well M90, showing that the correlation coefficient can meet the requirements of acoustic impedance inversion.

4.2. Interpretation of faults

After the calibration and interpretation of horizons, the next step is the interpretation of faults. In order to enhance the interpretation and the identification of small faults, three-instantaneous profiles (instantaneous amplitude, instantaneous frequency, and instantaneous phase) are used to make the breakpoints of small faults more clear and reliable, compared with the breakpoints interpreted by conventional profiles.

Firstly, two different dips in Inline and Crossline respectively were chosen to calculate the normalized energy, then the time - azimuth and time - dip were calculated. In order to make ant tracking better, previous processing of seismic data had been done. (1) Structure smoothing, a local smoothing with the guide of the input signal, enhancing the continuity of seismic reflection and filtering out noise, and (2) Chaotic processing, a method of estimating "organization destruction" with dip and azimuth to make strong amplitudes stronger and weak amplitudes weaker, and (3) Variance calculation, an estimation of the signal variance to reduce noise and the spatial discontinuity of seismic data was enhanced accordingly, and then the variance time slice for the obtained data was extracted (Fig. 9, A), and finally the ant body was extracted (Fig. 9, B). The key to secure the ant tracking algorithm is selecting the parameters. In this study, the appropriate parameters of the target formations were ultimately determined through repeated experiments. Secondly, Automatic Fault Extraction (AFE) was used to extract the fault pillars (Fig. 9, C) of the study area by setting the appropriate extraction parameters with active tracking algorithm, making the fault plane combination is more reasonable and breakpoints are more obvious. Finally, the 3D visual fault plane (Fig. 9, D) is established.

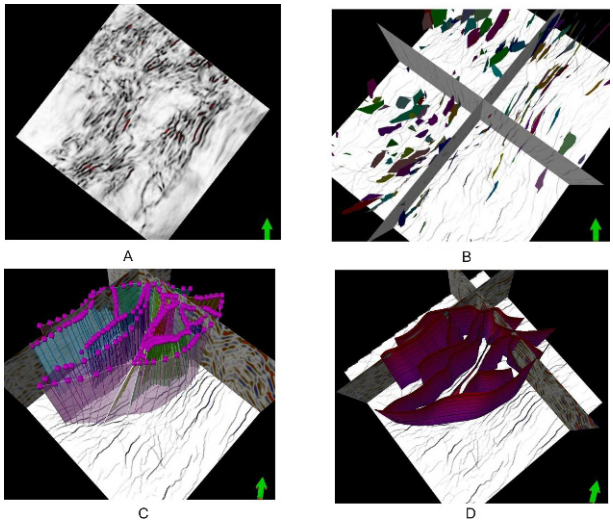

Figure 9. A: variance time slice; B: automatic extraction of ant body fault plane; C: 3D visualization of the main fault pillars in geological modeling area; D: 3D visualization of the main fault plane in the geological modeling area.

5. Detailed 3D Geological Modeling

Detailed 3D geological modeling is the basis for the static models of oilfields and it can be used as a predictive tool for the management and development of oilfields [21]. The well and seismic data have been combined, within a sequence stratigraphic framework, to construct a 3D geological model of the M1 block. In this study, the grid system for 3D geological modeling was established in a finer scale. The grid size was 20×20 m in the plane and 0.4 m in the vertical direction with a total grid block number of 1730190. A typical scale is generally 1m in vertical direction.

5.1. Fault modeling

Fault modeling defines the faults in the geological model which will provide the basis for generating the 3D grid. In the process of fault modeling, it is necessary to create Key Pillars along all the faults to incorporate them into the reservoir model; fault sticks can be used like fault polygons to create Key Pillars. Also, it is important to do some fine-tuning (such as digitizing or truncating pillars) on a specific key pillar or along the whole fault.

Taking the M1 block for example, we adhere to the following principles: (1) Fault traces at all mapped horizons were used to define the positions of the fault surfaces at depth; (2) Each fault surface was modeled as a 3D grid. With a comprehensive application of seismic data, drilling data and other static geological data based on detailed stratigraphic correlation and detailed structural interpretation, the original fault lines are obtained by digitizing structural maps and then fault pillars, which combine with fault points obtained from stratigraphic correlation to establish the original fault plane with fault polygons of different strata, followed by appropriate modifications of the fault planes. The final fault model (Fig. 10, A) is obtained after fine-tuning done on some fault points to make fault points accord with fault planes. The size of the editing window can be changed by changing the size of the shape point or horizon node that it represents. There are many cross-cutting faults in the study area, so the importance of having smooth transitions between connecting faults is to lay the ground for the pillar grid as orthogonal as possible. The smoother the transitions are, the better the precision of the grid system will be. Fig. 10, B shows the surface model on the premise of fault model and grid system.

5.2. Structural modeling

Structural modeling reflects the spatial distribution of reservoir strata [22], including fault modeling, pillar gridding, horizon modeling, etc. [23]. In this study, the step following fault modeling is subdivision of surface model. Ccross-cutting surfaces and fault planes divide the 3D model into lots of blocks with various shapes and different properties, and each block is output and endowed with the respective geological attributes in order to satisfy the following steps. After the adjustment of geological surfaces' morphology and relationships, blocks are extracted and then organized to form an integrated 3D geological body (Fig. 10, C). The structural modeling of the M1 block reproduces the three-dimensional distribution of the fault planes and the spatial spread of formation interfaces, and is more intuitive in reflecting local structure than by fence models (Fig. 10, D,E) and cross-well profiles (Fig. 10, F).

5.3. Sedimentary-microfacies modeling and property modeling

Sedimentary microfacies of the lower second sub-member consist of channel, proximal overbank, distal overbank and mud microfacies. And the upper third sub-member develops underwater distributary channel, mouth-bar, overbank and sand sheet. According to the provenance and reservoir characteristics of the M1 block, the bandwidth, angle and search radius are defined for different sedimentary microfacies, then the variogram curve, representing regional variable correlation, is obtained. Combined with the sedimentary microfacies plan map, the 3D sedimentary-microfacies model (Fig. 11, A) is built with Sequential Indicator Simulation. The result shows that 3D distribution of sedimentary microfacies has good consistency with their plan distribution by establishing 3D fence model and profiles. Longitudinal changes of sedimentary characteristics and provenance direction between layers, which can be seen from Fig. 11, B, contribute to a better understanding of the depositional environment changes and provide valuable guidance for property modeling.

The initial step of property modeling is data analysis, in which variogram parameters of each sedimentary microfacies are analyzed and adjusted according to their spatial distribution characteristics, and singular values corresponding with actual geology conditions are truncated to ensure the original property data (porosity and permeability) is within a reasonable range. The standard deviation is greatly reduced after transformation, which shows a reasonable enhancement of porosity data and permeability data for meeting the input requirements of property modeling. Property parameters of different sed-

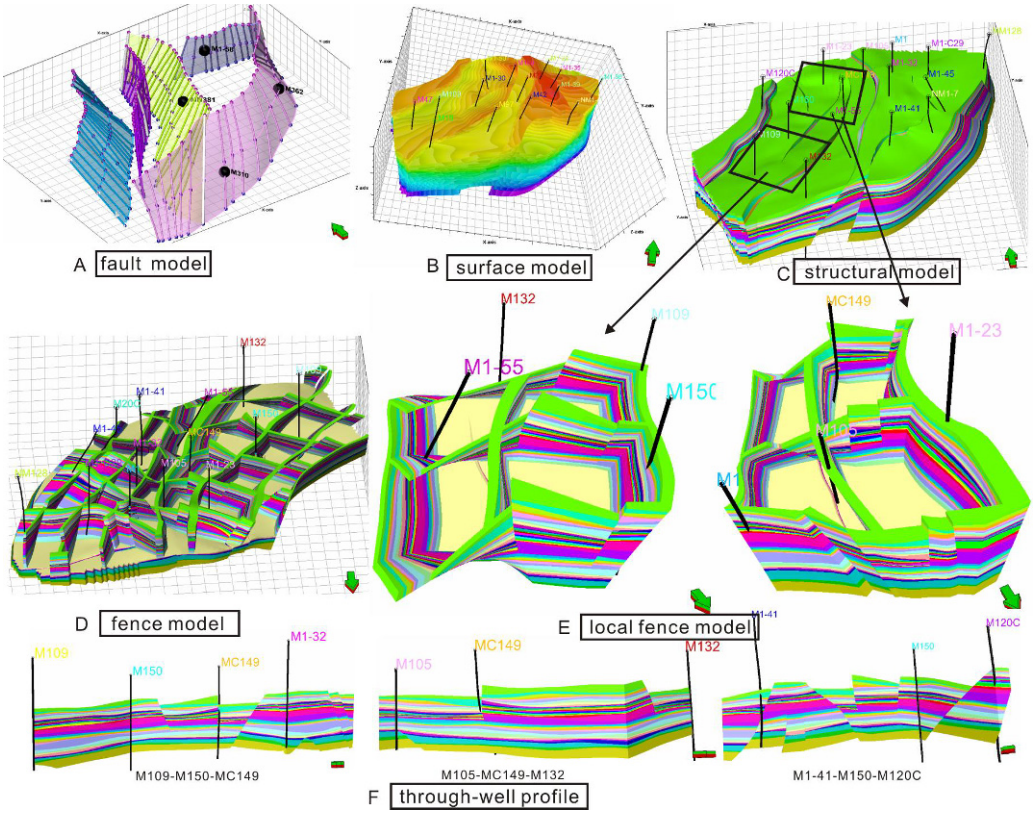

Figure 10. 3D geological model of the M1 block, showing the fault model and the structural model including the fence model and cross-well profile. A: The final fault plane modified with fault points and the fault plane accords with faults points; B: 3D visualization of surface model and fault model; C: 3D regional geological model of M1 block; D: Three dimensional structural fence model of (C) at X-axis (1, 1, 10) and Y-axis (1, 1, 15); E: Zoomed-in views of the two black boxes in (D), showing a detailed distribution pattern of structural model; F: Through well structural sections, showing the spatial stratigraphic distribution between wells in each layer.

imentary microfacies have different distributions in space. In addition, the spatial distribution of reservoir physical parameters has a certain randomness, so the use of sedimentary facies-controlled modeling in property modeling makes reservoir heterogeneity descriptions more accurate [24]. Based on this, the permeability model and the porosity model are established with Sequential Gaussian Simulation [25, 26]. In the lower second sub-member, the average porosity is 26% and the permeability ranges in $400 \times 10^{-3}\mu m^2$ to $1000 \times 10^{-3}\mu m^2$, belonging to high porosity and permeability reservoir. As to the upper third sub-member, the porosity is between 20% and 30%, and the permeability is generally larger than $100 \times 10^{-3}\mu m^2$, belonging to high porosity and medium-high permeability reservoir.

From 3D porosity model and permeability model and their profiles (Fig. 11, C-F) it can be seen that the simulated property values conform with actual reservoir property values, ranging from 10% to 35% for porosity and $30 \times 10^{-3}\mu m^2$ to $1500 \times 10^{-3}\mu m^2$ for permeability. In addition, the porosity distribution has good correlation with permeability. Under the control of sedimentary microfacies, the properties of the M1 block have roughly the same changing trend as sedimentary microfacies do, that property differences between sedimentary microfacies are reflected in the bedding planes, and sedimentary sequences and rhythmic changes are reflected in vertical section. High property values are mainly distributed in the northwest, the northeast and the center of the study area, in the same direction as the provenance, indicating a high reliability of property data analysis and a guarantee for later numerical simulation accordingly.

6. Conclusions

(1) Three types of interfaces are identified through core examination that are the erosion surface, the bedding change interface and the thickness cyclic changing interface of sandstone and mudstone. These are the reliable basis for the division of sequence cycles, and three sequence orders in the stratigraphic architecture of M1 block

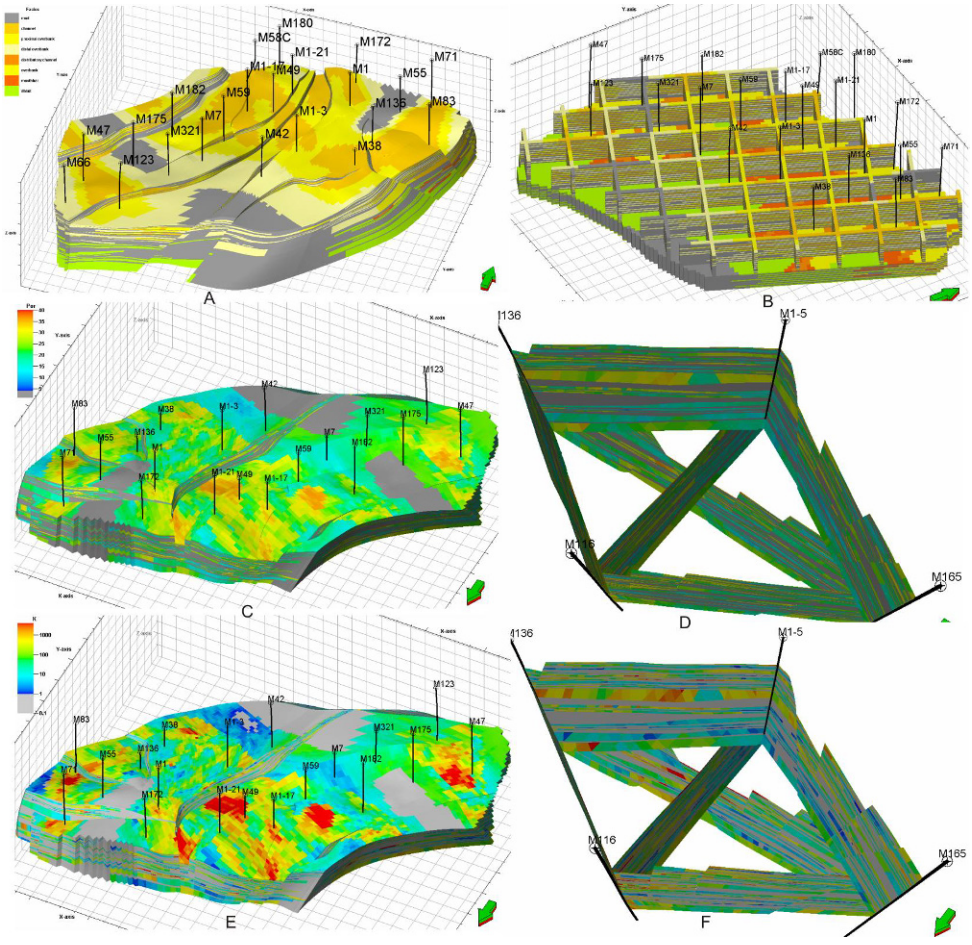

Figure 11. Sedimentary-microfacies model and property model of the M1 block. A: 3D reginal sedimentary-microfacies model of M1 block, established with Sequential Indicator Simulation; B: Regional sedimentary-microfacies fence model without fault at X-axis (1,1,10) and Y-axis (1,1,10); C: 3D regional porosity model established with facies-controlled modeling; D: Multiple-well porosity profile of well M136 - well M1-5 - well M165 - well M116; E: 3D regional permeability model established by facies-controlled modeling; F: Multiple-well permeability profile of well M136 - well M1-5 - well M165 - well M116.

are divided: fifth-order (V), fourth-order (IV) and third-order (III); and they are subdivided into thirty-two short-term cycle sequences, eight mid-term cycle sequences and two long-term cycle sequences for the lower second sub-member and the upper third sub-member of Shahejie Formation.

(2) High-resolution isochronous stratigraphic correlation framework is established based on well-logging characteristic and entropy spectral analysis. The result shows that the lower second sub-member is a positive depositional sequence indicating a transgression process, while, the upper third sub-member is a negative depositional sequence indicating a regression process.

(3) Based on structural interpretation, an integrated 3D geological model of the M1 block has been established. The reservoir parameter distribution is based on logging data of well point and core analysis, also, physical property between wells has been predicted by establishing a property model. The sedimentary microfacies model and the property model of the M1 block have good consistency with actual geological information and accurately reflect the geological construction.

Acknowledgments

This study was supported by Specialized Research Fund for the Doctoral Program of Higher Education (No. 20110003110014). The authors wish to thank SINOPEC Zhongyuan Petroleum Exploitation Bureau Geoscience Institute for supplying research data.

References

[1] Mitchum R. M., Seismic stratigraphy and global changes of sea-level, part11: glossary of terms used in seismic stratigraphy. In: Payton, C. E. (Ed.), Seismic Stratigraphy: Applications to Hydrocarbon Exploration, AAPG, 1977, 26, 205–212

[2] Octavian C., Patrick G. E., The sequence stratigraphic concept and the Precambrian rock record: an example from the 2.7–2.1 Ga Transvaal Supergroup, Kaapvaal craton. Precambrian Research, 1999, 97, 215-251

[3] Karen S. H., Roberto L., John W. N., Three-dimensional structural modeling of multi-valued salt masses. Workstation Presentations, 2005, 3, 2058-2060

[4] Raper J., Key 3D modeling concepts for geoscientific analysis, in A.Turner, ed., Three-dimensional modelling with geoscientific information systems, NATO ARW, Santa Barbara, CA, 1989

[5] Yu X. H., Oil/gas Reservoir Sedimentary of Clasolite Series. Petroleum Industry Express, Beijing, 2002

[6] Wang G. H., Liu Z. L., Li Q. Y., Fine structure interpretation and reservoir prediction of Wenmingzhai Oilfield—a case of S2 reservoir for M1 block, Geophysical Prospecting for Petroleum, 2011, 50, 165-172 (in Chinese).

[7] Cross T. A., Lessenger M. A., Sediment Volume Partitioning: Rational for Stratigraphic Model Evaluation and High-Resolution Stratigraphic Correlation. In: Gradstein, F. M., Sandvisk, K. O., Milton, N. J., eds., Sequence Stratigraphy Concepts and Applications. NPF Special Publication, 1998, 8, 171–195

[8] Galloway W. E., Genetic Stratigraphic Sequences in Basin Analysis I: Architecture and Genesis of Flooding-Surface Bounded Depositional Units. AAPG Bulletin, 1989, 73, 125–142

[9] Vail P. R., Seismic Stratigraphy and Global Changes of Sea-Level. In: Payton, C. E., ed., Seismic Stratigraphy Applications to Hydrocarbon Exploration. Am. Assoc. Pet. Geol. Mem., 1977, 26, 49–212

[10] Izart A., Briand C., Vaslet D., Vachard D., Coquel R., Maslo A., Stratigraphy and sequence stratigraphy of the Moscovian in the Donets basin. Tectonophysics, 1996, 268, 189-209

[11] Deng H. W., Wang H. L., Li X. Z., The identification and correlation technology of base-level of sequence stratigraphy and its application. Journal of Oil & Gas Geology, 1996, 17, 177-184 (in Chinese).

[12] Deng H.W., Wang H.L., Zhu Y. J., The principle and application of high resolution sequence stratigraphy. The Geological Publishing House, Beijing, 2002

[13] Shi N., Fine times division of sand gravel body of the upper fourth submember of Shahejie Formation in Yanjia-Yong'an area. Master's Thesis, Ocean University of China, China, 2009

[14] Jiang Y.M., Sedimentary Facies in the Second Member of Dainan Formation, the South Slope, Gaoyou Sag. Master's Thesis, Ocean University of China, 2008 (in Chinese)

[15] Cross T. A., High-resolution stratigraphic correlation from the perspective of base-level cycles and sediment accommodation. In: Proceedings of Northwestern Europian Sequence Stratigraphy Congress, 1994, 105-123

[16] Cross T. A., Lessenger M. A., Sediment volume partitioning: Rationale for stratigraphic model evolution and high-resolution stratigraphic correlation. Norwegian Petroleums-Forening Conference, 1996

[17] Zhen R. C., Yin S. M., Peng J., Sedimentary dynamics analysis of base-level cycle structure and superposition style. Acta Sedimentologica Sinica, 2000, 18, 369-375 (in Chinese).

[18] Zhen R. C., Peng J., Wu C. R., Sub-division of base level cycle of continental basin and the significance. Acta Sedimentologica Sinica, 2001, 19, 249-255 (in Chinese).

[19] Li G. F., Liao Q. J., Wang S. X., Yuan S. Q., Wang S. D., Issues of horizon calibration by synthetic seismograms. Geophysical Prospecting For Petroleum, 2008, 47, 145-149

[20] Zhang J. L., Shen F., Lai Z.Y., Study of Reservoir Geology and Reservoir Characterization. Northwest University Press. Xi'nan, China. 1993

[21] Freulon X. C., Dunderdale I. D., Integrating Field Measurements With Conceptual Models To Produce a Detailed 3D Geological Model. Society of Petroleum Engineers 28877, 1994. 99-108

[22] Wu Y. B., Zhang Y. T., Wu Z. G., The 3D visualization of the reservoir modeling based on Petrel, Special Oil and Gas Reservoirs, 2007, 15, 21-24

[23] Durlofsky L. J., Milliken W. J., Bernath A., Scaleup in the Near-Well Region, Society of Petroleum Engineers, 2000, 5, 110-117

[24] Zhang J. L., Li X., Wang J. K., Application of Facies-controlled Modeling Technology: a case study of H54-H98 block. The 2nd Conference on Environmental Science and Information Application Technology, 2010, 603-606

[25] Chen F. X., The application of variogram in predicating braided river sandstone reservoir scale[J], Journal of Chongqing Science and Technology, 2008, 10, 9-11 (in Chinese)

[26] Guo K., Shi J., Variogram law study of Donghe sandstone reservoir in Tazhong 4 block, 2008, 4, 4-8 (in Chinese)